Electronic Supplementary Information

Unassisted Photoelectrochemical Hydrogen Peroxide Production over MoO_x-Supported Mo on Cu_3BiS_3 Photocathode

Subin Moon,[1] Young Sun Park, [1] Hyungsoo Lee,[1] Wooyong Jeong, [1] Eunji Kwon,[2] Jeongyoub Lee,[1] Juwon Yun,[1] Soobin Lee, [1] Jun Hwan Kim,[1] Seungho Yu,[2] and Jooho Moon*[1]

[1] Department of Materials Science and Engineering, Yonsei University, Seoul 03722, Republic of Korea

[2] Energy Storage Research Center, Korea Institute of Science and Technology 5, Hwarang-ro- 14-gil, Seongbuk-gu, Seoul 02792, Republic of Korea

* E-mail: jmoon@yonsei.ac.kr

Keywords: photoelectrochemical oxygen reduction reaction, strength of adsorbate adsorption, metal oxide supported catalyst, unassisted hydrogen peroxide production

Supplementary Figures

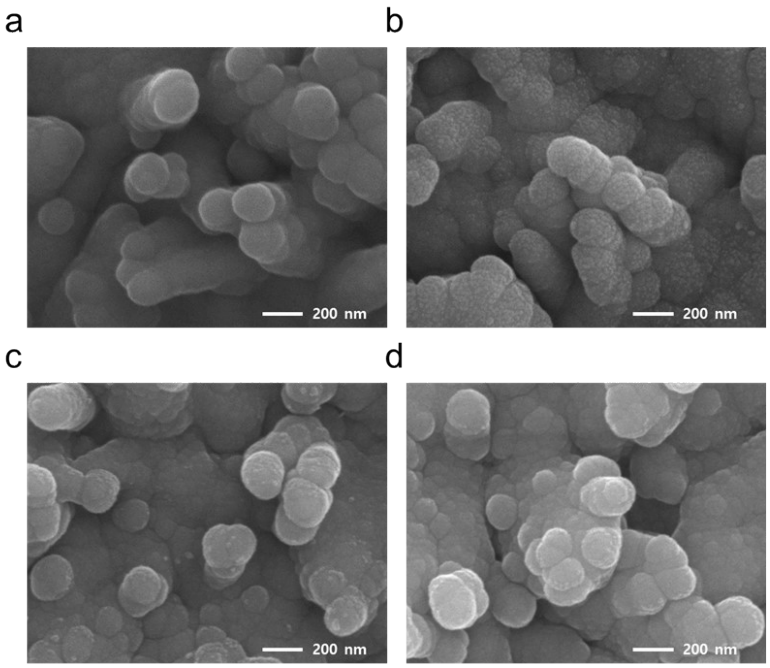

Fig. S1 Top-view scanning electron microscopy image for a) $Cu_3BiS_3/CdS/TiO_2$, b) $Cu_3BiS_3/CdS/TiO_2/MoO_x$, c) $Cu_3BiS_3/CdS/TiO_2/MoO_x/Mo$, and d) $Cu_3BiS_3/CdS/TiO_2/Mo$.

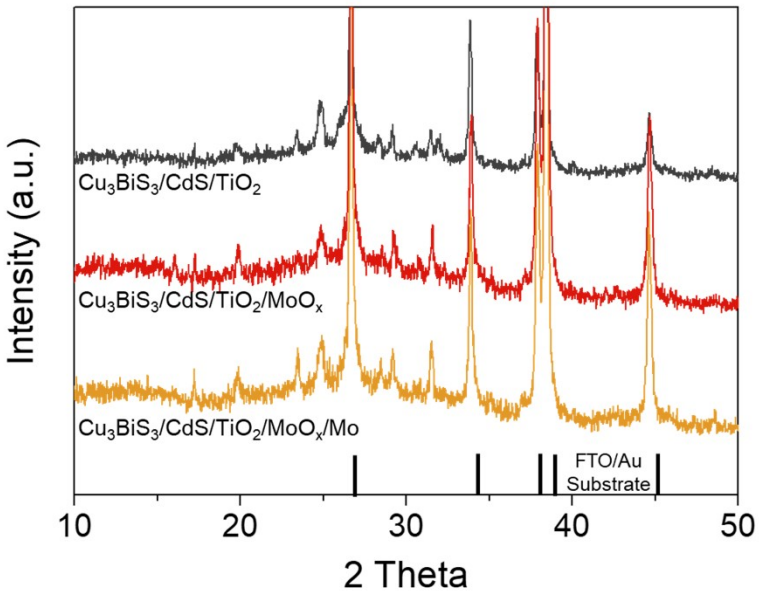

Fig. S2 XRD patterns for $Cu_3BiS_3/CdS/TiO_2$ (black) and after MoO_x deposition (red) followed by Mo deposition (yellow).

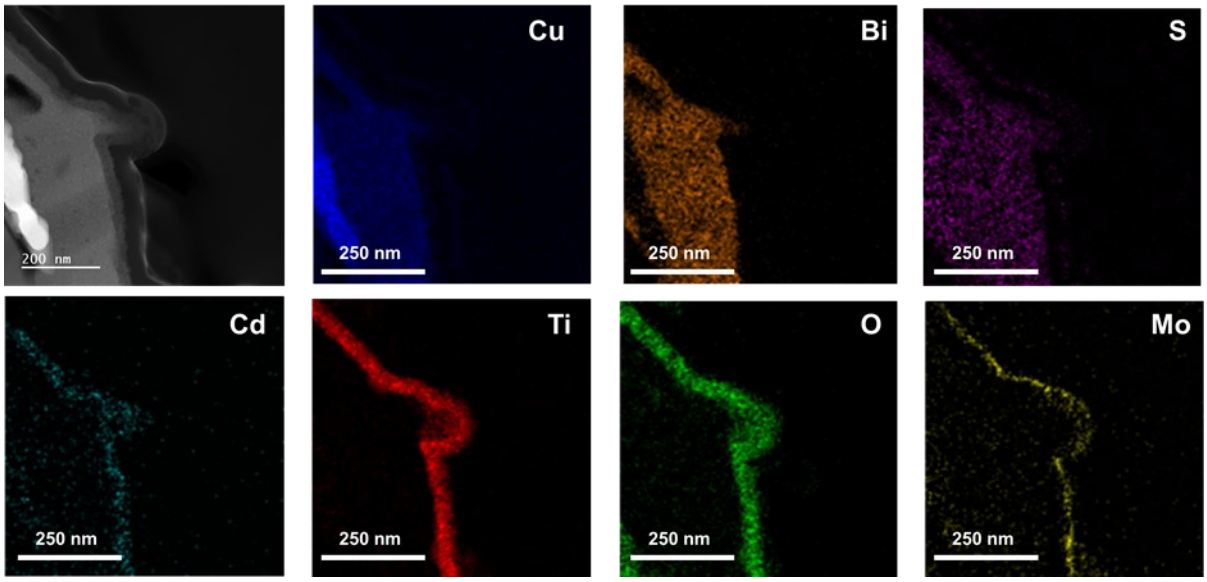

Fig. S3 TEM image and corresponding EDS elemental mapping images at the low magnification for $Cu_3BiS_3/CdS/TiO_2/MoO_x/Mo$.

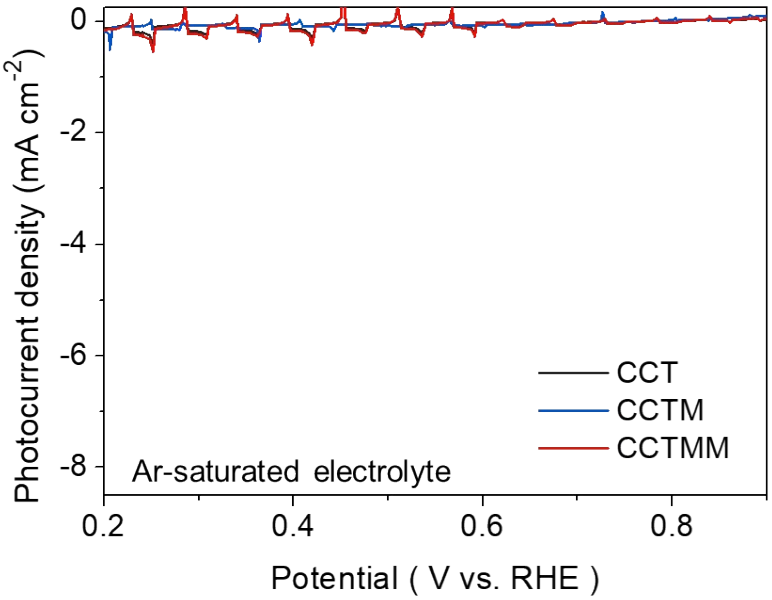

Fig. S4 LSV measurements for CCT, CCTM, and CCTMM photocathodes under 1-sun solar simulated AM 1.5 G irradiation in an Ar-saturated 0.2 M KOH electrolyte (pH 12).

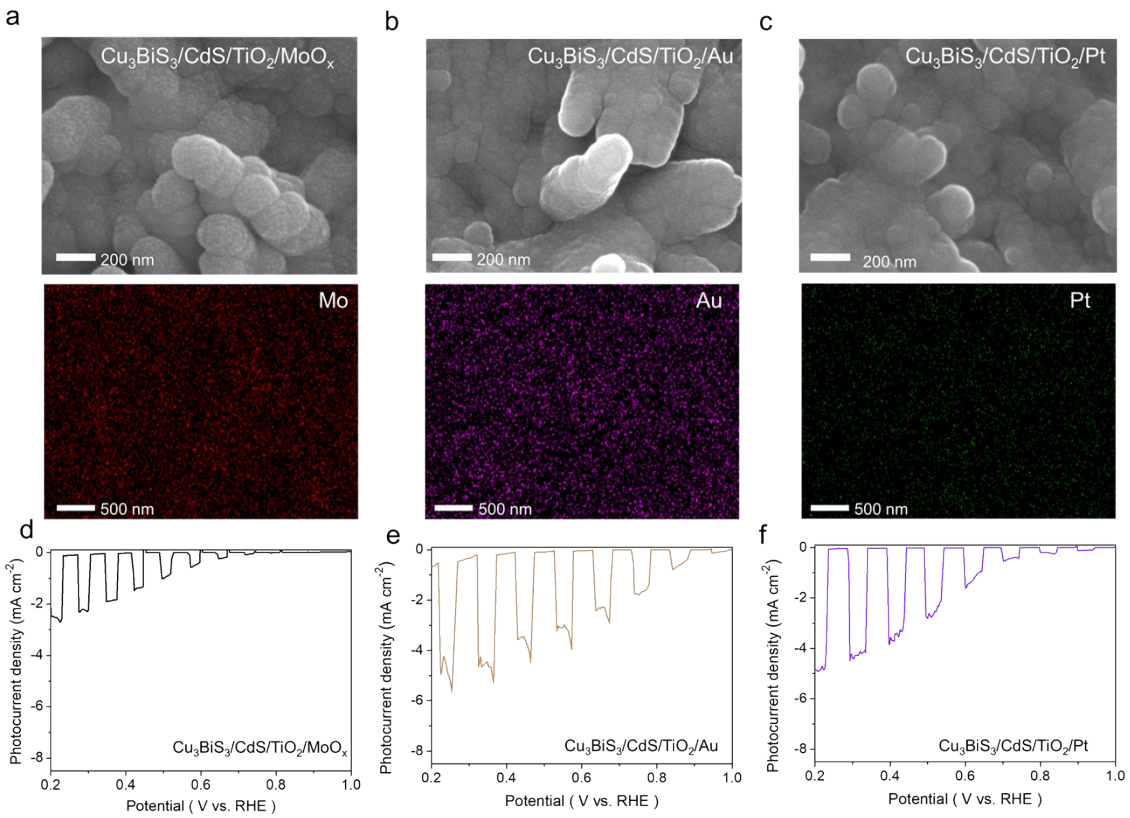

Fig. S5 SEM images, EDS mapping, and LSV measurements for a,d) $Cu_3BiS_3/CdS/TiO_2/MoO_x$, b,e) $Cu_3BiS_3/CdS/TiO_2/Au$ and c,f) $Cu_3BiS_3/CdS/TiO_2/Pt$.

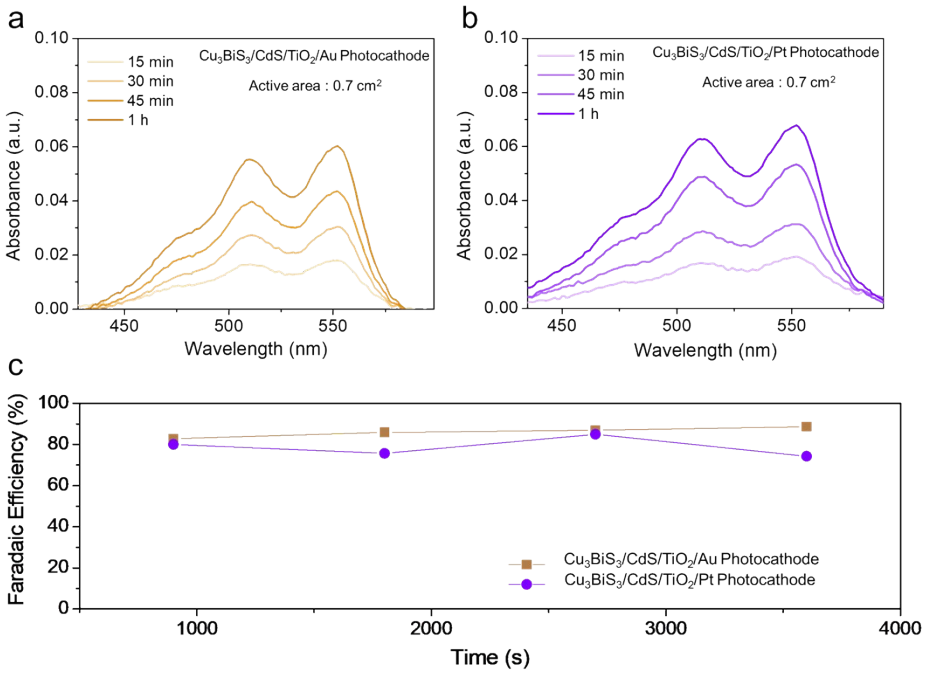

Fig. S6 Time-dependent absorption spectra of the catholyte aliquot as a function of the reaction duration for a) $Cu_3BiS_3/CdS/TiO_2/Au$ and b) $Cu_3BiS_3/CdS/TiO_2/Pt$ photocathodes. c) Faradaic efficiency of the photocathodes.

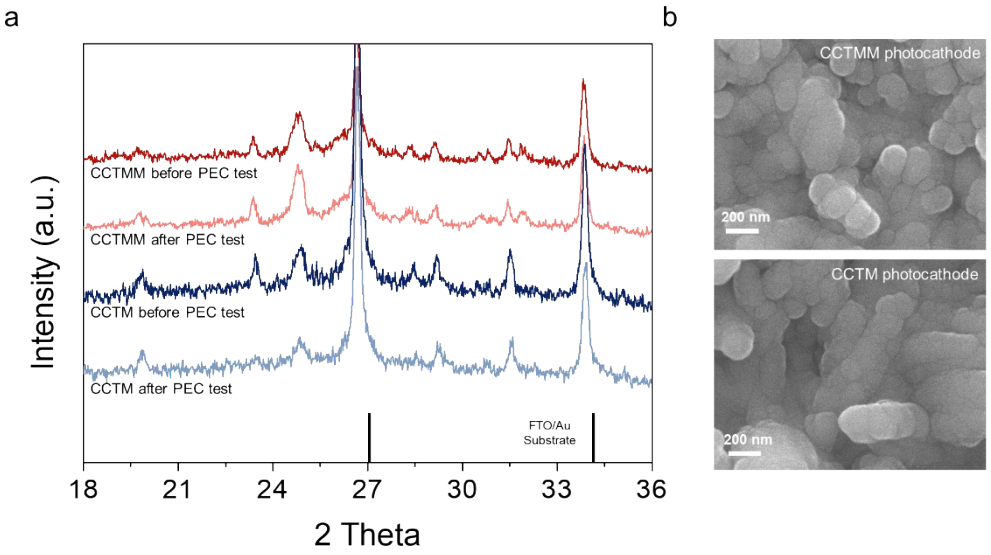

Fig. S7 a) XRD patterns for CCTM and CCTMM photocathodes of before and after stability test. b) Top-view SEM images for CCTM and CCTMM photocathodes of after stability test.

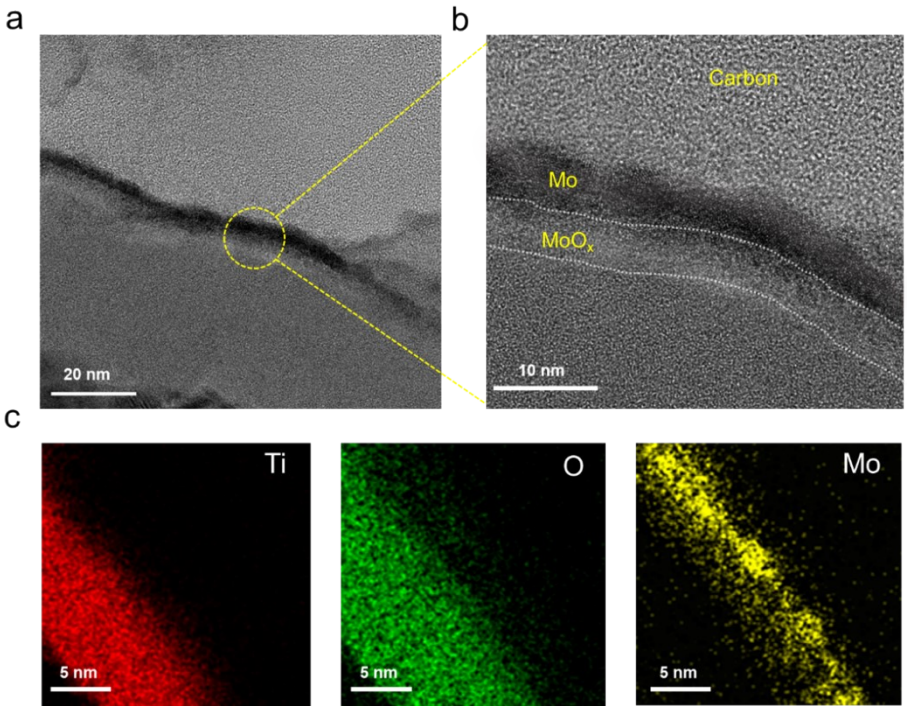

Fig. S8 a) Cross-sectional TEM image, b) HR-TEM cross-sectional image, and c) EDS mapping of CCTMM photocathode after stability test.

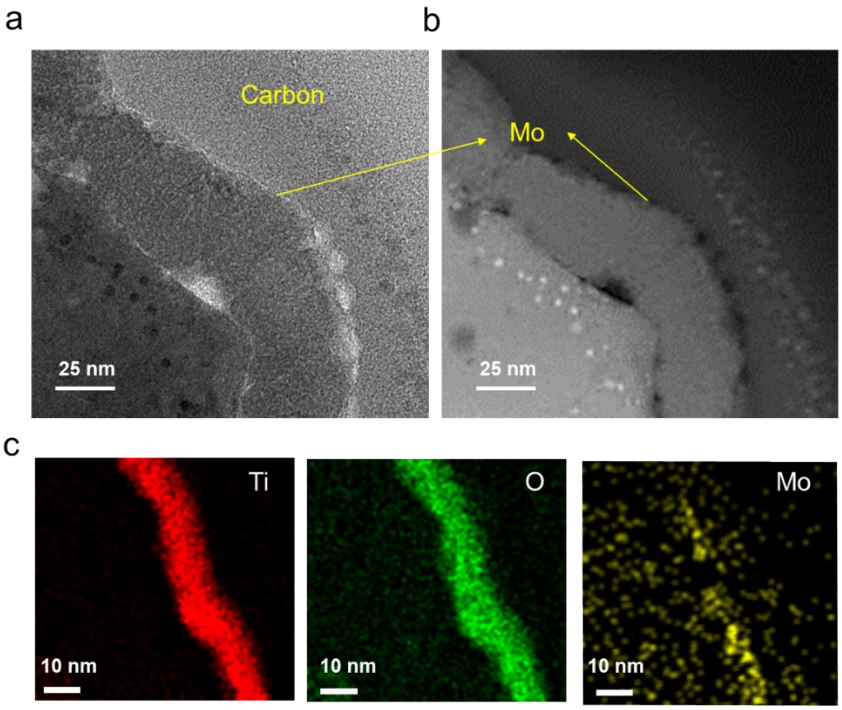

Fig. S9 a) Bright-field, b) dark-field TEM images, and c) EDS mapping of CCTM photocathode after PEC test.

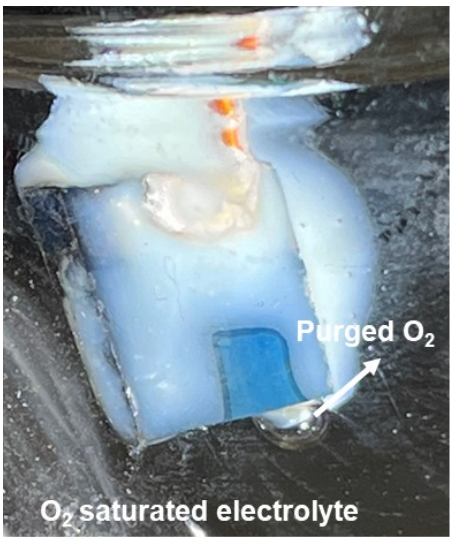

Fig. S10 Photograph of the CCTMM photocathode being operating in an O_2-saturated 0.2 M KOH electrolyte.

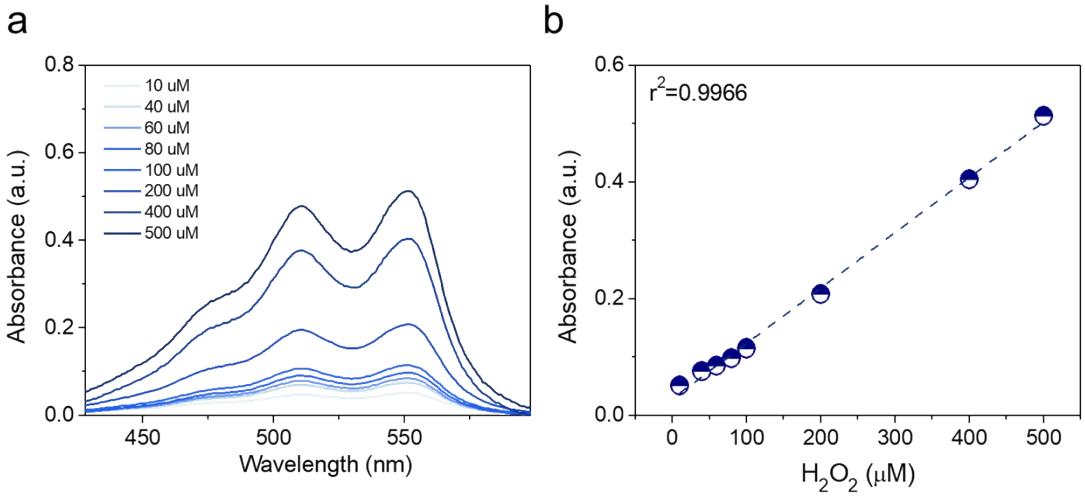

Fig. S11 a) Absorbance as a function of the added amount of H_2O_2. A calibration curve is derived based on the absorbance at 551 nm using the colorimetric method. b) Resulting calibration curve as a function of the H_2O_2 content.

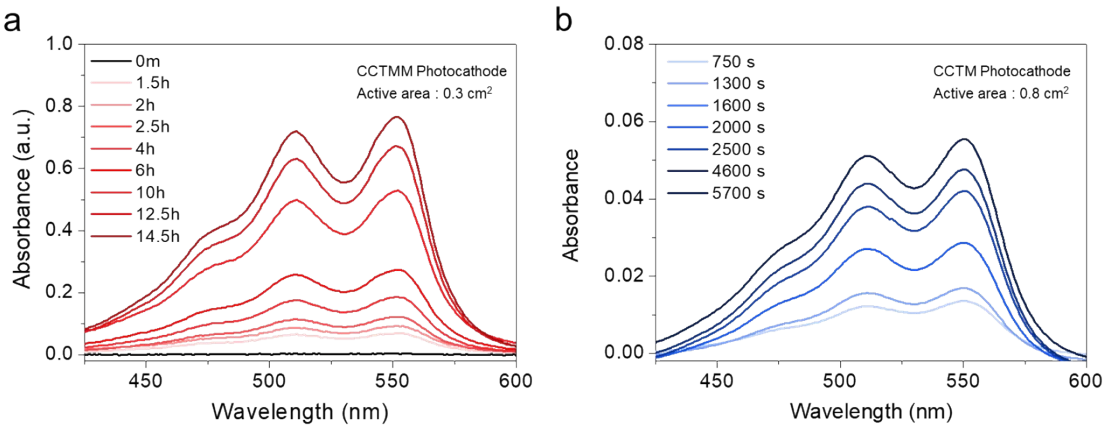

Fig. S12 Time-dependent absorption spectra of the catholyte aliquot as a function of the reaction duration for the a) CCTMM and b) CCTM photocathodes.

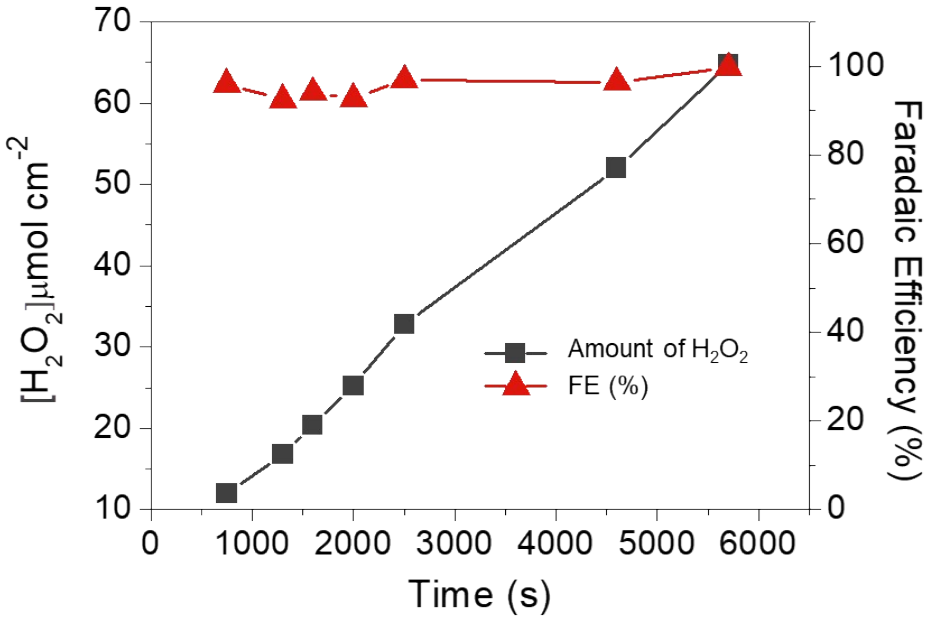

Fig. S13 Amount of generated H_2O_2 and Faradaic efficiency (FE) of operating CCTM photocathode.

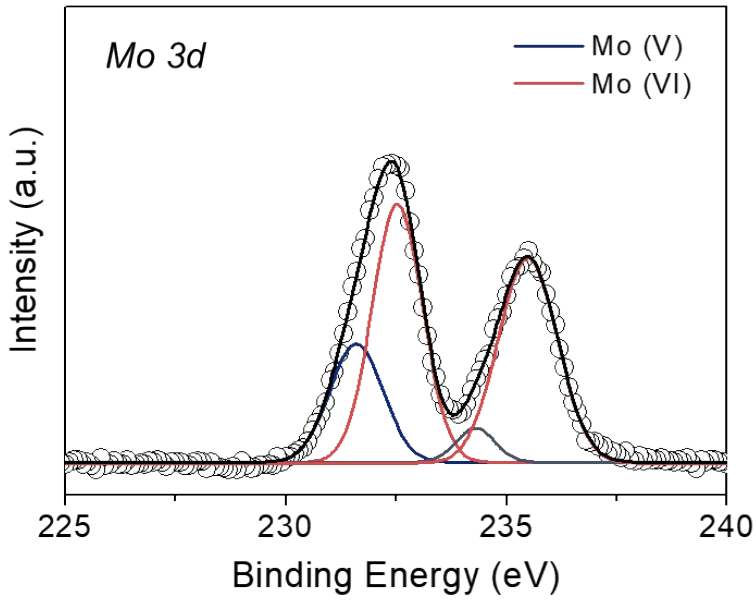

Fig. S14 XPS spectra for Mo 3*d* of the MoO_x.

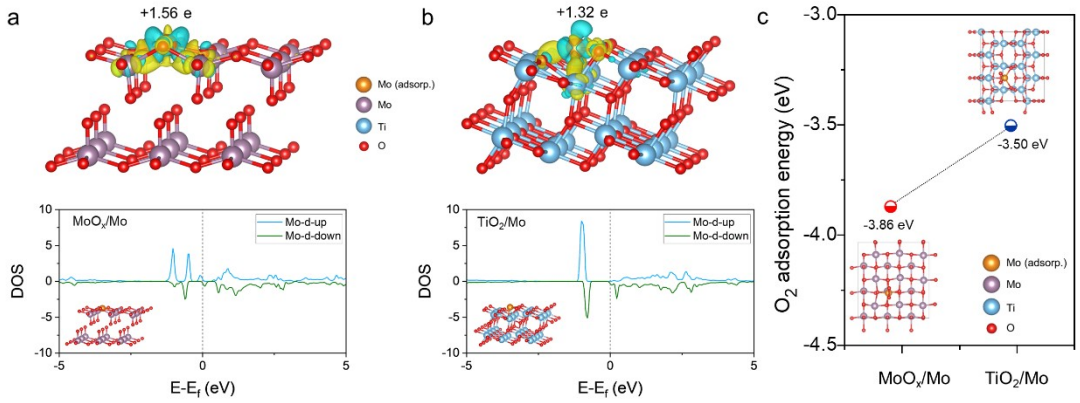

Fig. S15 Differential charge density, Bader charge analysis, and the partial density of states (PDOS) for Mo d orbital of the a) MoO_x/Mo and b) TiO_2/Mo structures. c) Adsorption energies of oxygen adsorbates on the MoO_x/Mo and TiO_2/Mo structures.

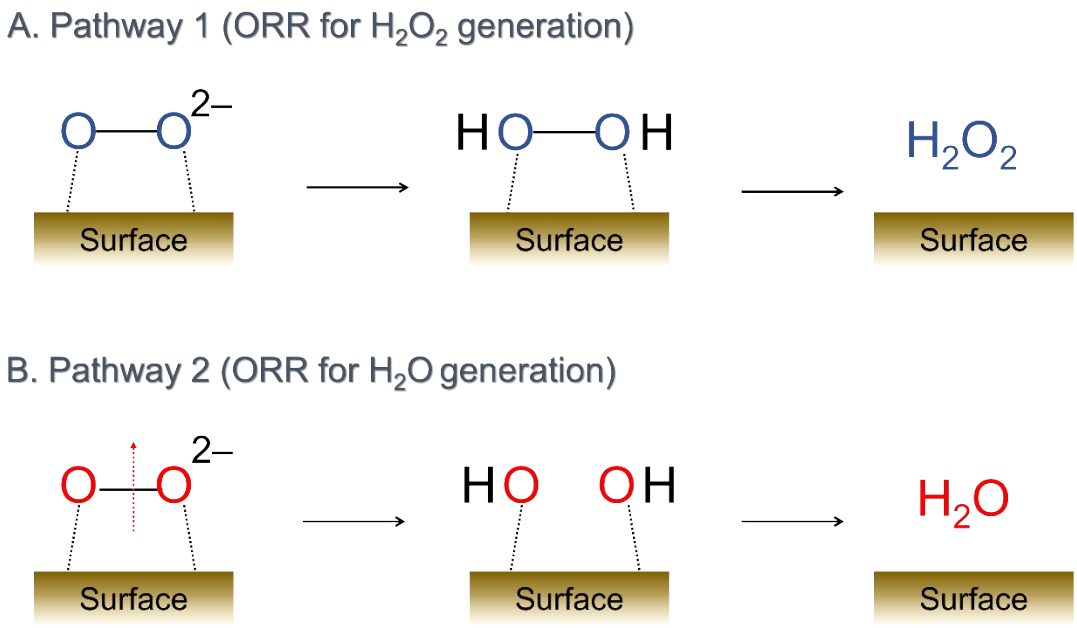

Fig. S16 Schematic illustrating the mechanisms of H_2O_2 production and H_2O generation. Pathway 1 is the case when E_d is larger than the threshold value of 3.5 eV, resulting in O–O preservation. Pathway 2 is when E_d is smaller than the threshold value of 3.5 eV. Excessive adsorption strength inevitably leads to the undesired production of H_2O instead of H_2O_2 by facilitating O–O bond cleavage in the oxygen-containing adsorbate.

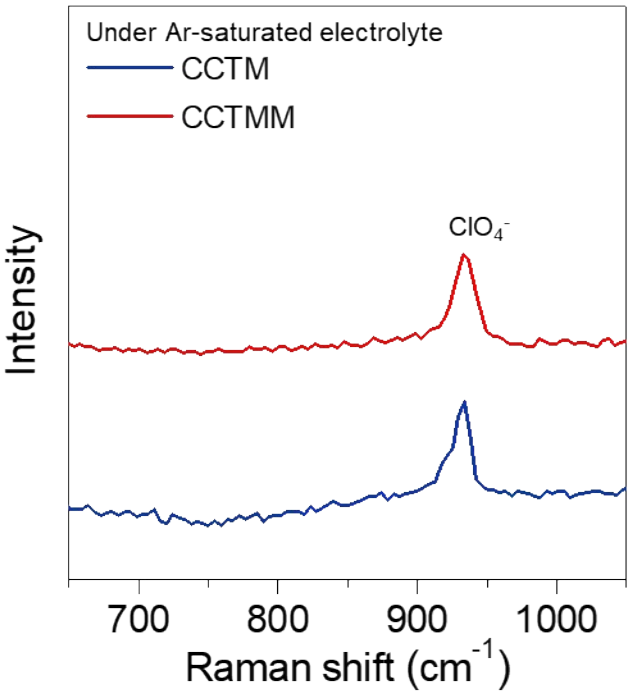

Fig. S17 *In situ* Raman spectra obtained during ORR over the CCTM and CCTMM photocathodes in Ar-saturated 0.1 M $NaClO_4$ electrolyte under 1-sun solar simulated AM 1.5 G irradiation at 0.6 V_{RHE}.

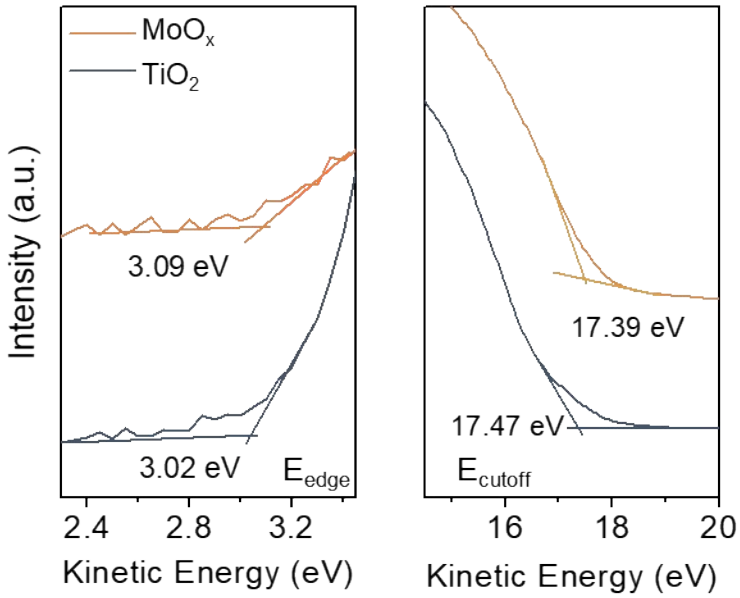

Fig. S18 Normalized UPS spectra of the valence band edge and secondary electron cutoff region for MoO_x and TiO_2.

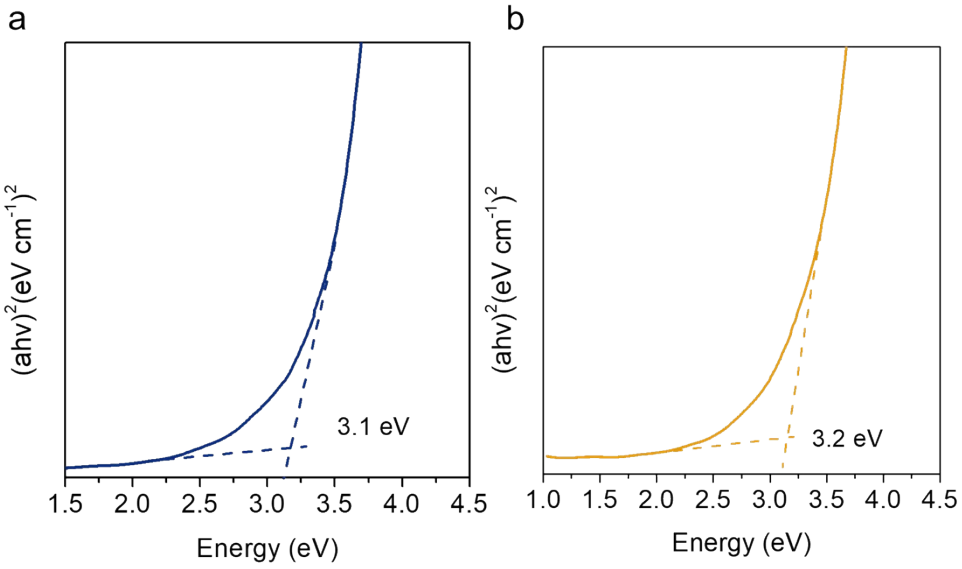

Fig. S19 Tau plots of a) TiO_2 and b) MoO_x deposited on bare FTO for determining the band gap.

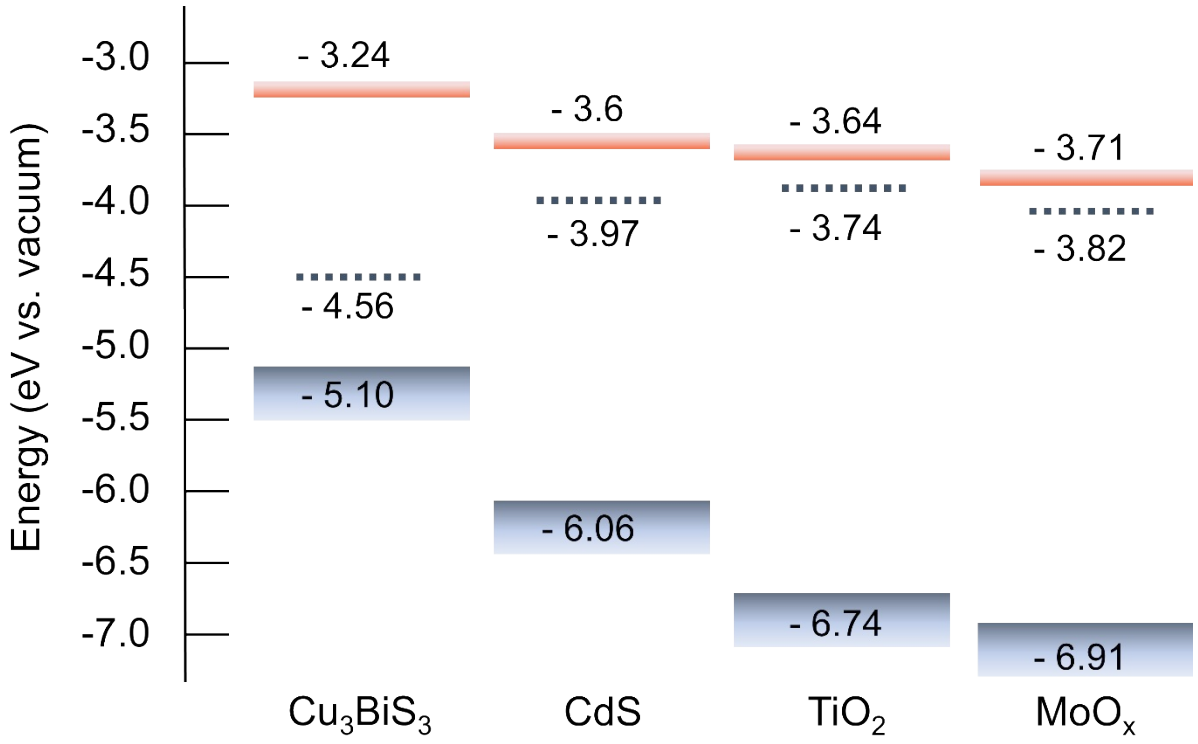

Fig. S20 Schematic band diagram of Cu_3BiS_3/CdS/TiO_2/MoO_x showing the relative energy positions based on the investigated band gaps of TiO_2 (3.1 eV) and MoO_x (3.2 eV).[S1-2] Band structures of Cu_3BiS_3 and CdS were obtained from our previous report.[S3]

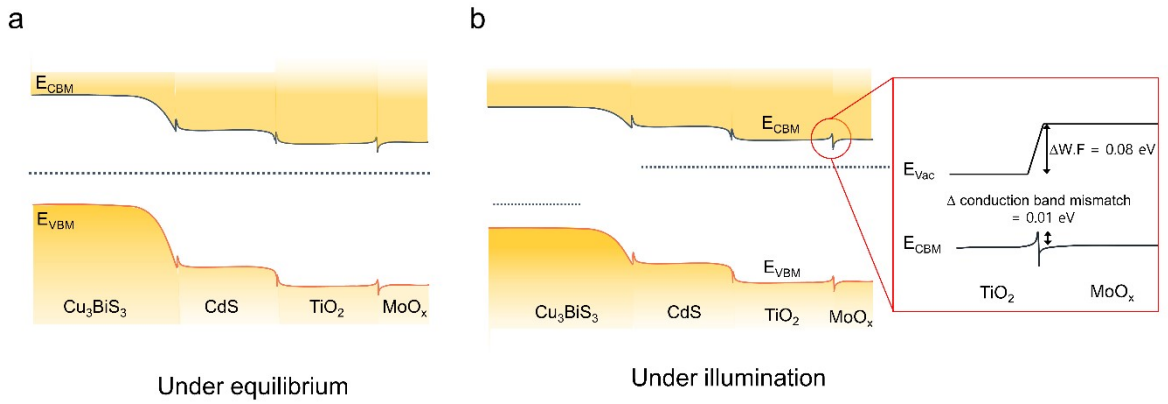

Fig. S21 Schematic band diagram of Cu_3BiS_3/CdS/TiO_2/MoO_x after junction formation a) under equilibrium and b) under illumination.

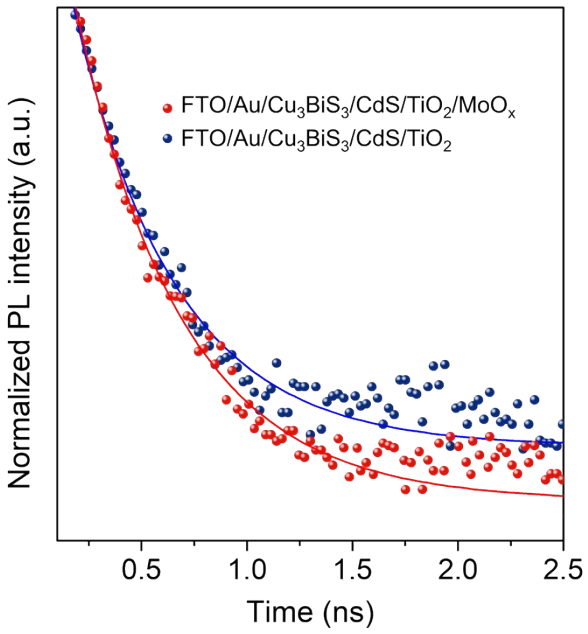

Fig. S22 TRPL graph for FTO/Au/Cu_3BiS_3/CdS/TiO_2 and FTO/Au/Cu_3BiS_3/CdS/TiO_2/MoO_x.

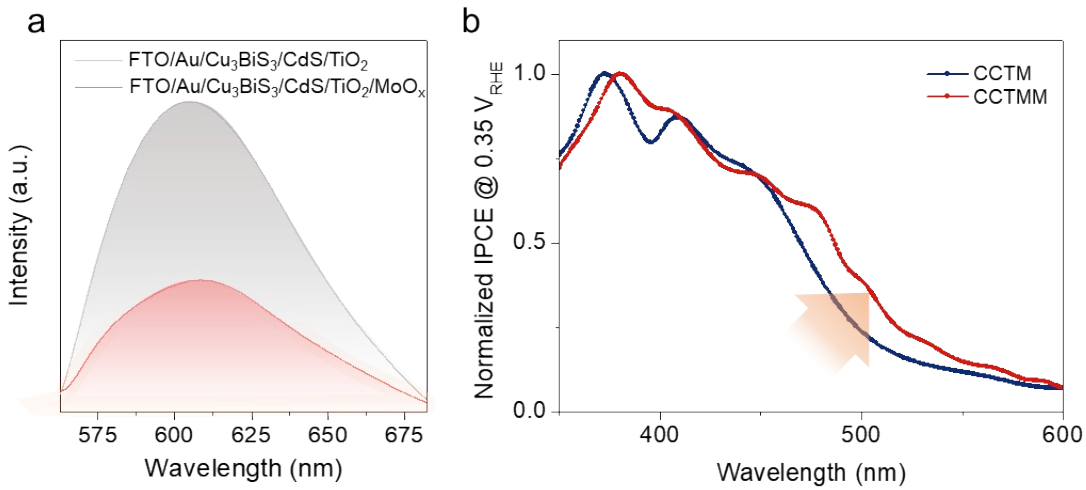

Fig. S23 a) Steady-state PL spectra for FTO/Au/Cu_3BiS_3/CdS/TiO_2 (grey) and after deposition of MoO_x (red). b) Normalized IPCE spectra for CCTM and CCTMM photocathodes under long wavelength regions (> 450 nm).

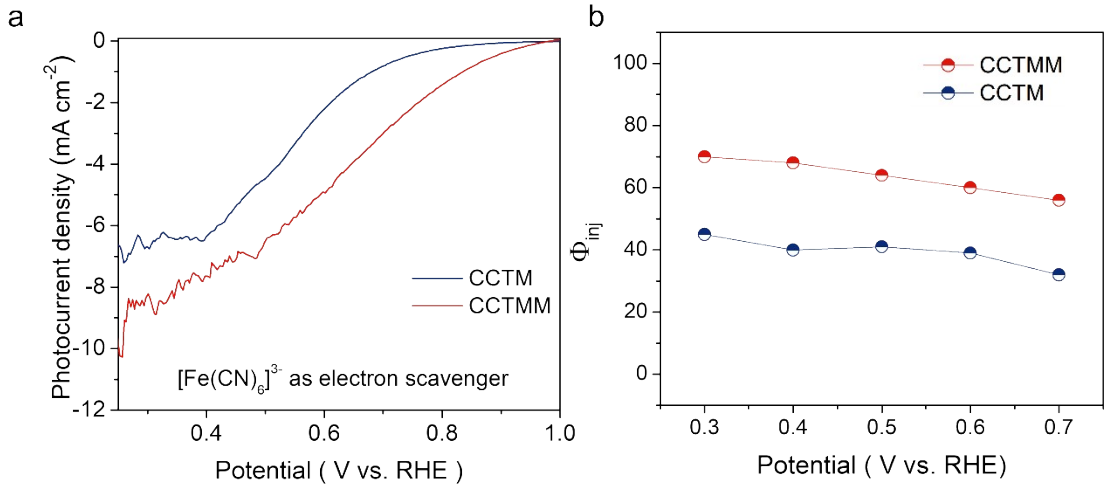

Fig. S24 a) J-V curves and b) charge injection efficiency of CCTM and CCTMM photocathodes under AM 1.5 G irradiation in 0.2 M KOH electrolyte with 0.05 M $K_3[Fe(CN)_6]$ as an electron scavenger.

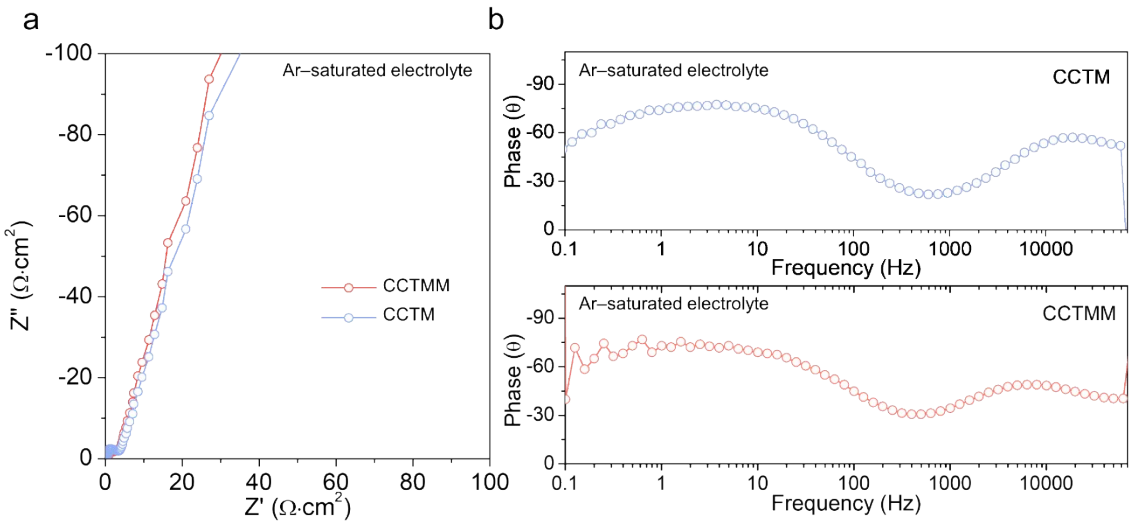

Fig. S25 a) Nyquist plot and b) Bode plot obtained from EIS measurements for CCTM and CCTMM photocathodes under 1-sun solar simulated AM 1.5 G irradiation in Ar-saturated 0.2 M KOH electrolyte.

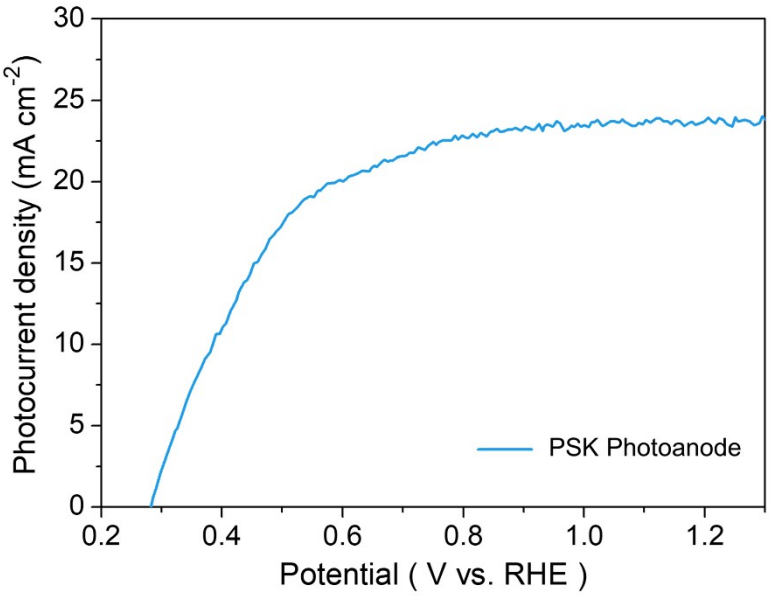

Fig. S26 LSV measurement for the PSK photoanode under 1-sun solar simulated AM 1.5 G irradiation in 0.2 M KOH electrolyte (pH 12).

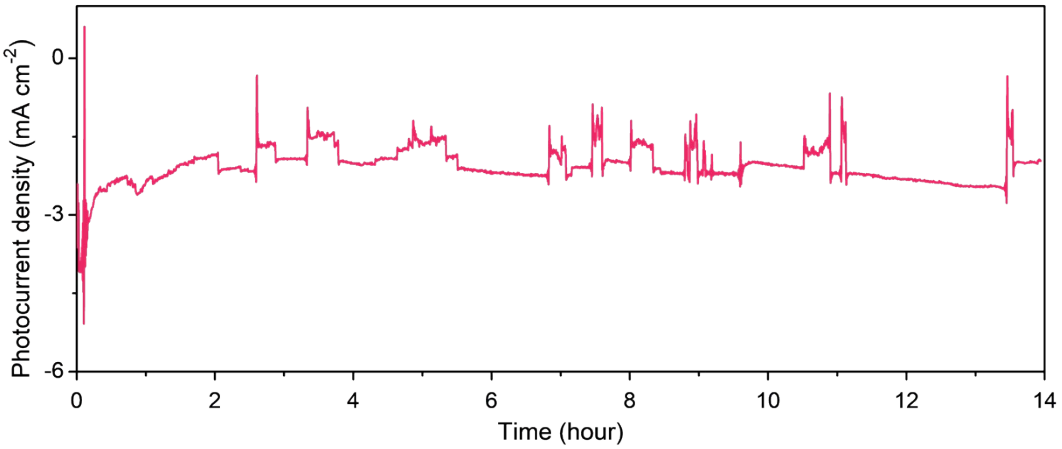

Fig. S27 Photocurrent density versus time curve for the unbiased CCTMM photocathode−PSK based photoanode coplanar configuration under 1-sun solar simulated AM 1.5 G irradiation.

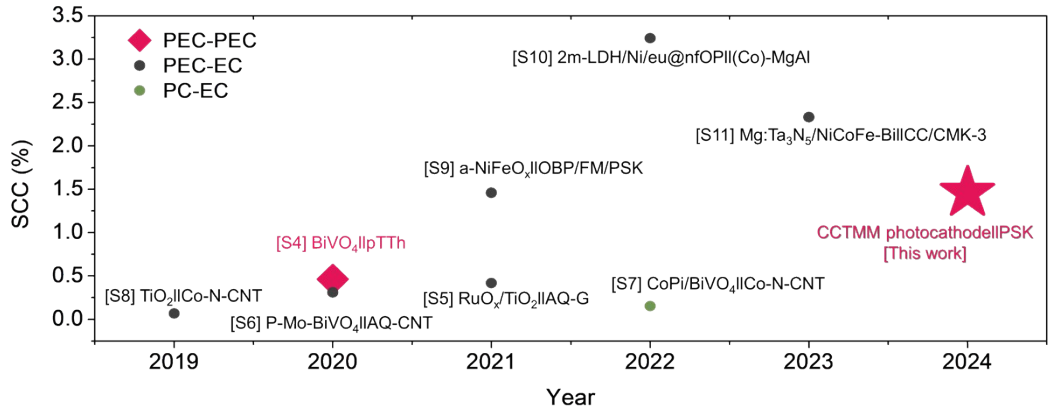

Fig. S28 Summary of SCC efficiency for bias-free photoelectrochemical H_2O_2 production cells without any assistant agent such as HCO_3^-.[S4-S11]

Table S1. Inductively coupled plasma (ICP) analysis result for the dissolved Mo concentration in the electrolyte during the device operation.

Sample	Concentration (ppb)	Relative standard deviation (%)
CCTM	30.005	0.7
CCTMM	7.035	1.30

Table S2. Non-radiative lifetime (τ_1) and radiative lifetime (τ_2) of the FTO/Au/Cu_3BiS_3/CdS/TiO_2 and FTO/Au/Cu_3BiS_3/CdS/TiO_2/MoO_x.

	τ_1 (ns)	τ_2 (ns)
FTO/Au/Cu_3BiS_3/CdS/TiO_2	0.55	1.1
FTO/Au/Cu_3BiS_3/CdS/TiO_2/MoO_x	0.49	0.61

Table S3. Area-specific resistance values and CPEs obtained by deconvolving the EIS spectra at 0.35 V_{RHE}.

sample	R_s (Ω)	R_{HF} (Ω cm^2)	CPE_{HF} (F S^{n-1} cm^2)	R_{LF} (Ω cm^2)	CPE_{LF} (F S^{n-1} cm^2)
CCTM	1.9	5.42	5.045×10^{-6} (n=0.881)	28	7.5×10^{-5} (n=0.933)
CCTMM	2.755	5.06	1.777×10^{-5} (n=0.811)	9.7	1.1×10^{-4} (n=0.895)

Supplementary Information References

S1. M. Hannula, H. Ali- Ali-Löytty, K. Lahtonen, E. Sarlin, J. Saari, M. Valden, Chem. Mater. 2018, **30**, 1199.

S2. D. J. Borah, A. T. T. Mostako, P. K. Saikia, P. Dutta, Mater. Sci. Semicond. Process. 2019, **93**, 111.

S3. S. Moon, J. Park, H. Lee, J. W. Yang, J. Yun, Y. S. Park, J. Lee, H. Im, H. W. Jang, W. Yang, J. Moon, *Adv. Sci.*, 2023, **10**, e2206286.

S4. W. J. Fan, B. Q. Zhang, X. Y. Wang, W. G. Ma, D. Li, Z. L. Wang, M. Dupuis, J. Y. Shi, S. J. Liao, C. Li, *Energy. Environ. Sci.*, 2020, **13**, 238.

S5. T. H. Jeon, B. Kim, C. Kim, C. Xia, H. T. Wang, P. J. J. Alvarez, W. Choi, *Energy. Environ. Sci.*, 2021, **14**, 3110.

S6. T. H. Jeon, H. Kim, H.-i. Kim, W. Choi, *Energy. Environ. Sci.*, 2020, **13**, 1730.

S7. M. Ko, Y. Kim, J. Woo, B. Lee, R. Mehrotra, P. Sharma, J. Kim, S. W. Hwang, H. Y. Jeong, H. Lim, S. H. Joo, J. W. Jang, J. H. Kwak, *Nat. Catal.*, 2022, **5**, 37.

S8. M. Ko, L. T. M. Pham, Y. J. Sa, J. Woo, T. V. T. Nguyen, J. H. Kim, D. Oh, P. Sharma, J. Ryu, T. J. Shin, S. H. Joo, Y. H. Kim, J. W. Jang, *Nat. Commun.*, 2019, **10**, 5123.

S9. R. Mehrotra, D. Oh, J. W. Jang, *Nat. Commun.*, 2021, **12**, 6644.

S10. J. Song, J. M. Yu, J. H. Ahn, H. Cho, J. Oh, Y. S. Kim, J. Kim, M. Ko, S. H. Lee, T. J. Shin, H. Y. Jeong, C. Yang, J. H. Lee, J. W. Jang, S. Cho, *Adv. Funct. Mater.*, 2022, **32**, 2110412.

S11. D. Zhu, C. Feng, Z. Y. Fan, B. B. Zhang, X. Luo, Y. B. Li, *Sustain. Energ. Fuels*, 2023, **7**, 3326.